Ferromagnetic resonance in ferromagnetic/ferroelectric Fe ⁄ Ba Ti O 3 ⁄ Sr Ti O 3 (001)

Chengtao Yu, Michael J. Pechan, Swedesh Srivastava, Chris J. Palmstrøm, Michael Biegaslski, Charles Brooks, and Darrell Schlom

Articles you may be interested in

Properties of ferroelectric/ferromagnetic thin film heterostructures
J. Appl. Phys. **115**, 17D713 (2014); 10.1063/1.4865316

Probing ferromagnetic/ferroelectric interfaces via spin wave resonance
Appl. Phys. Lett. **102**, 042404 (2013); 10.1063/1.4789761

Magnetoelectric coupling in a ferroelectric/ferromagnetic chain revealed by ferromagnetic resonance
J. Appl. Phys. **113**, 013908 (2013); 10.1063/1.4772746

Structural, magnetic and electrical properties of ferromagnetic/ferroelectric multilayers
J. Appl. Phys. **109**, 123920 (2011); 10.1063/1.3598134

Electric-field control of ferromagnetic resonance in monolithic BaFe 12 O 19 – Ba 0.5 Sr 0.5 TiO 3 heterostructures
J. Appl. Phys. **108**, 043911 (2010); 10.1063/1.3467777

Ferromagnetic resonance in ferromagnetic/ferroelectric Fe/BaTiO$_3$/SrTiO$_3$(001)

Chengtao Yu[a)] and Michael J. Pechan
Department of Physics, Miami University, Oxford, Ohio 45056, USA

Swedesh Srivastava and Chris J. Palmstrøm
Department of Chemical Engineering and Materials Science, University of Minnesota-Minneapolis, Minnesota 55455, USA

Michael Biegaslski, Charles Brooks, and Darrell Schlom
Materials Science and Engineering, Penn State University, University Park, Pennsylvania 16802, USA

Single Fe(001) films (30 nm thick) have been epitaxially grown on ferroelectric BaTiO$_3$/SrTiO$_3$(001) substrates at different growth temperatures to study the mutual interaction between the multiferroic components. This paper reports on the as-grown magnetic properties of the structures as a precursor to a full investigation of the multiferroic interactions. Ferromagnetic resonance measurements were carried out at 36 GHz cavity and variable frequency microstrip resonators. Dual resonance modes are observed in the film, which are attributed to relaxed Fe in the film interior and strained Fe at the interface. Fourfold anisotropy is present for both modes with energy density consistent with that of bulk Fe. The interface mode is characterized by a large out-of-plane anisotropy comparable and opposite in sign to the shape anisotropy. This strained interfacial Fe should serve to couple the multiferroic components in this system. Dispersion curves show both optic and acoustic branches along the hard axis [110], with the optic branch resulting from resonance below saturation, indicating high quality Fe in these samples. Growth temperature has minimal influence on the observed anisotropy energies. © *2008 American Institute of Physics*. [DOI: 10.1063/1.2834243]

INTRODUCTION

Given the mix of electric and magnetic influences in modern electronics, the multiferroic effect,[1] which involves one or more of ferroelectric, ferromagnetic, and ferroelastic materials, has been the subject of considerable recent interest.[2,3] Novel multiferroic materials[4] including artificial layered structures[5] consisting of different ferroic components are of particular interest.[6] Herein we report on the static and dynamic magnetic properties of as-grown, epitaxial ferromagnetic Fe films on ferroelectric BaTiO$_3$/SrTiO$_3$(001) buffer/substrates.

EXPERIMENTAL

A series of Fe (30 nm) films has been epitaxially grown on a BaTiO$_3$(100 nm)SrTiO$_3$(001) buffer/substrate by molecular beam epitaxy at different temperatures (20, 100, 200, and 350 °C). X-ray data showed single crystal (001) oriented growth except for T_g=350 °C, where there exist two domains, (001) and (211). Structure data show that all the Fe films are relaxed. Atomic force microscopy measurements revealed island morphology with larger islands and deeper valleys with increasing growth temperature. Magnetization loops are measured with conventional vibrating sample magnetometry, and ferromagnetic resonance (FMR) measurements were performed in a 36 GHz cavity and on a variable frequency microstrip device.

III. RESULTS AND DISCUSSION

Figure 1 shows magnetization loops along [110] and [100] for the sample grown at 20 °C. The loop displays a hard-axis saturation field of approximately 640 Oe, consistent with values for bulk single crystal Fe.[7] Results for the other samples are similar, with slight variation in the 350 °C sample due to the twinned Fe.

The in-plane anisotropy is best determined by FMR at 36 GHz, where the magnetization is aligned with the field at all angles. These data, shown in Fig. 2 for the sample grown
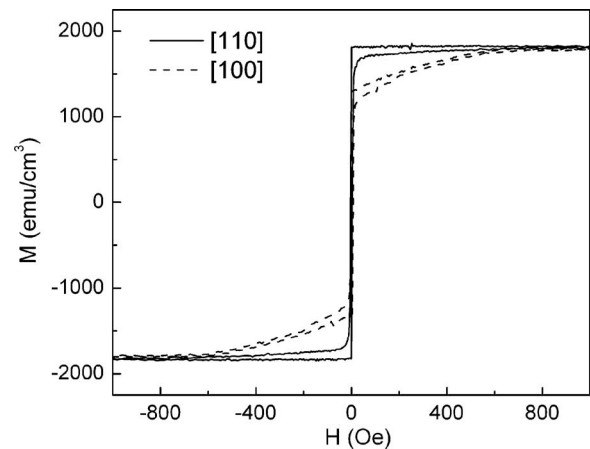
FIG. 1. Magnetization hysteresis loops along [110] and [100] for an Fe/BaTiO$_3$/SrTiO$_3$ film grown at 20 °C.

[a)]Electronic mail: yuc@muohio.edu.
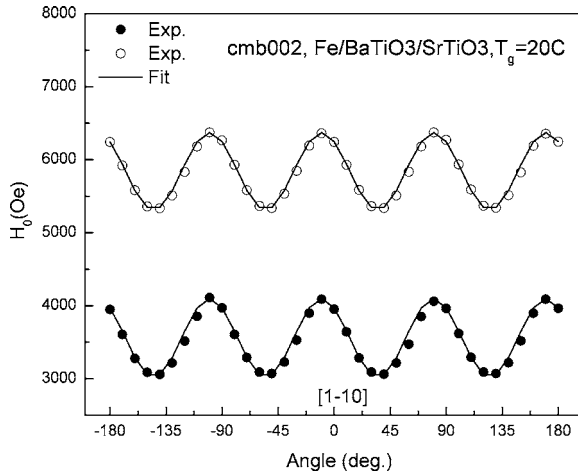
FIG. 2. Typical ferromagnetic resonance field as a function of in-plane angle. The solid lines are fits to the data based on a model described in the text. Both film interior and interface modes show fourfold anisotropy comparable to bulk Fe.

TABLE I. Magnetic anisotropy data derived from 35 GHz resonance for samples grown at different temperatures for both interior and interface modes.

T_g (°C)	20	100	200	350
	Interior mode			
K_4 (10^5 erg/cm^3)	1.35	1.31	1.3	1.3
K_u (10^6 erg/cm^3)	1.9	2.1	2.2	1.9
	Interface mode			
K_4 (10^5 erg/cm^3)	1.23	1.2	1.2	1.22
K_u (10^7 erg/cm^3)	−1.37	−1.3	−0.93	−1.1

at 20 °C, reveals two resonances, each showing a simple fourfold anisotropy with peak-to-peak amplitude of approximately 1000 Oe. Also shown in the figure are the fits, based on the Landau–Lifshitz equation of motion,[8] using the energy expression

$$E = -MH[\sin\theta\cos(\phi-\phi_H)] - (2\pi M^2 + K_u)\sin^2\theta$$
$$+ K_4\sin^2 2\phi\sin^2\theta, \tag{1}$$

where the first term is the Zeeman energy ($M=1700$ emu/cm^3) ϕ and ϕ_H are the azimuthal angles that M and H make with the easy axis, respectively, and θ is the out-of-plane angle; the second is the out-of-plane shape anisotropy with K_u the additional out-of-plane term; the third is the in-plane fourfold anisotropy energy. The resonance equation is derived from the following well-known expression:[9]

$$\left(\frac{\omega}{\gamma}\right)^2 = \frac{1}{(M\sin\theta)^2}\left[\frac{\partial^2 E}{\partial\theta^2}\frac{\partial^2 E}{\partial\phi^2} - \left(\frac{\partial^2 E}{\partial\theta\partial\phi}\right)^2\right], \tag{2}$$

yielding, for the stated energy and assuming saturation ($\phi = \phi_H$),

$$\left(\frac{\omega}{\gamma}\right)^2 = \left[H + \frac{8K_4}{M}\cos 4\phi_H\right]$$
$$\times\left[\left(H + \frac{K_4}{M}(\cos 4\phi_H - 1) + 4\pi M + \frac{2K_u}{M}\right]. \tag{3}$$

The fit, using K_4 and K_u as adjustable parameters, gives the first order fourfold anisotropy constants of 1.35×10^5 and 1.23×10^5 ergs/cm^3 for the two peaks, respectively, which are consistent with that of bulk single crystal Fe (Ref. 10) (1.05×10^5 ergs/cm^3). The additional out-of-plane anisotropy values, K_u, are 1.9×10^6 ergs/cm^3 (10% of $4\pi M$) and -1.37×10^7 ergs/cm^3 (75% of $4\pi M$) for the film interior and interface, respectively. This small peak with large out-of-plane anisotropy likely arises from strained Fe at the interface with the ferroelectric material. This strained Fe promises to provide the desired coupling between the multiferroic components in the system. Results for samples grown at el-

evated temperatures of 100, 200, and 350 °C are shown in Table I. The anisotropy values derived from the two modes for all samples are comparable, indicating no appreciable influence of growth temperature on magnetic properties of both the Fe film and interface.

Measurements were made as a function of frequency to map out the frequency/field dispersion relation. Representative raw spectra (along the hard [110] axis) and angular data are shown in Fig. 3. At 15 GHz one mode is observed whose in-plane angular dependence is distorted relative to that observed at 36 GHz by the nonsaturation of M with field around the hard direction. Below approximately 11 GHz, two modes are observed in the [110] direction. These modes merge with decreasing frequency, until the resonance disappears entirely below approximately 7 GHz. The angular dependence of the high field mode becomes increasingly peaked around [110] with decreasing frequency, which again is due to resonance far from saturation. Interestingly, at low frequencies (7.5 GHz in Fig. 3), the angular range for observing resonance is extremely narrow. The two modes merge within 5° of the hard axis and disappear altogether beyond that. The dual-mode behavior can be understood if one observes the dispersion curves in both the easy and hard in-plane directions shown in Fig. 4. Acoustic-type modes are observed for both easy- and hard-axis resonances, but below the saturation field (approximately 640 Oe) an optic-type mode is observed along the hard axis. This latter mode arises from resonance in the unsaturated state as observed in other single crystal systems[11,12] and as demonstrated in the following model. Below the saturation field in the hard direction, the assumption $\phi = \phi_H$ made in obtaining Eq. (3) must be relaxed. Prior to determining the resonance condition, the equilibrium in-plane angle (ϕ) of the magnetization must be obtained and is given, in the case of Eq. (1), by the transcendental equation

$$\frac{2K_4}{M}\sin 4\phi = H\sin(\phi-\phi_H). \tag{4}$$

The resonance about each equilibrium position is evaluated using Eq. (2), yielding
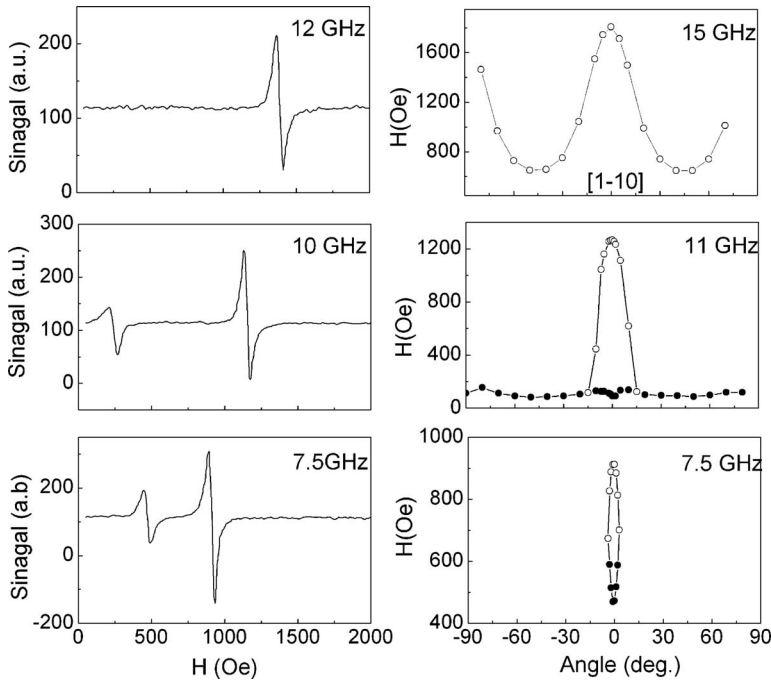
FIG. 3. Left row: ferromagnetic resonance spectra at different low microwave frequencies measured on a microstrip. Right row: angular dependence of resonance field at low frequencies.

$$\left(\frac{\omega}{\gamma}\right)^2 = \left[H\cos(\phi - \phi_H) + \frac{8K_4}{M}\cos 4\phi \right]$$
$$\times \left[\left(H\cos(\phi - \phi_H) + \frac{K_4}{M}(\cos 4\phi - 1) + 4\pi M \right. \right.$$
$$\left. \left. + \frac{2K_u}{M} \right]. \right. \tag{5}$$

The calculated dispersions along [100] (ϕ_H=0) and [110] (ϕ_H=45) are plotted in Fig. 4 as solid lines, showing close agreement with the data. The hard-axis calculations required a 2° misalignment between ϕ_H and the hard-axis direction to best fit the data. It has been shown that the sharpness of the dispersion curve minimum at the hard-axis saturation is extremely sensitive to such misalignments.[13] The sharp angular dependence in the dual mode region at low frequencies is a result of this extreme sensitivity. The observed dispersion explains the existence of a dual-mode resonance along the

hard direction in a well-defined frequency range and a single mode at higher frequencies. Dispersion curves obtained from samples grown at 100, 200, and 350 °C did not differ substantially from that displayed in Fig. 4.

In summary, we have demonstrated that high quality, single crystal Fe has been grown epitaxially on ferroelectric $BaTiO_3/SrTiO_3$(001) with magnetic properties closely approximating those of bulk Fe. In addition, it appears that the interfacial Fe is modified from that in the interior, potentially providing the desired coupling between the multiferroic components in the system. This characterization forms the foundation upon which future investigations of magnetoelectric effects will be undertaken.

FIG. 4. Dispersion curves along the easy axis [100] (open circles) and hard axis [110] (closed circles). Lines indicate calculations based on a model described in the text.

[1] W. Eerenstein, N. D. Mathur, and J. F. Scott, Nature (London) **442**, 759 (2006).
[2] M. Fiebig, J. Phys. D **38**, R123 (2005).
[3] M. I. Bichurin, V. M. Petrov, O. V. Ryabkov, S. V. Averkin, and G. Srinivasan, Phys. Rev. B **72**, 060408 (2005); M. I. Bichurin, V. M. Petrov, Yu. V. Kiliba, and G. Srinivasan, *ibid.* **66**, 134404 (2002).
[4] Y. Yamasaki, H. Sagayama, T. Goto, M. Matsuura, K. Hirota, T. Arima, and Y. Tokura, Phys. Rev. Lett. **98**, 147204 (2007).
[5] M. K. Lee, T. K. Nath, C. B. Eom, M. C. Smoak, and F. Tsui, Appl. Phys. Lett. **77**, 3547 (2000).
[6] Y. Bai, J. Zhou, Z. Gui, L. Li, and L. Qiao, J. Appl. Phys. **101**, 083907 (2007).
[7] L. C. Cullity, *Introduction to Magnetic Materials*, Addison-Wesley, 1972.
[8] For example, R. L. Compton, M. J. Pechan, S. Maat, and E. E. Fullerton, Phys. Rev. B **66**, 054411 (2002); M. J. Pechan, N. Teng, J. Stewart, J. Z. Hilt, E. E. Fullerton, J. S. Jiang, C. H. Sowers, and S. D. Bader, J. Appl. Phys. **87**, 6686 (2000); C. Yu, M. J. Pechan, and G. J. Mankey, Appl. Phys. Lett. **83**, 3948 (2003).
[9] J. Smit and H. C. Beljers, Philips Res. Rep. **10**, 1113 (1955).
[10] C. Kittel, *Introduction to Solid State Physics* (Wiley, New York, 1986).
[11] R. H. Kingston and P. E. Tannenwald, J. Appl. Phys. **29**, 232 (1958).
[12] A. Layadi, Phys. Rev. B **66**, 184423 (2002).
[13] C. Yu, M. J. Pechan, B. Ryan, J. Katine, L. Folks, and M. Carey, J. Appl. Phys. **101**, 09D118 (2007).